

PAPER

[View Article Online](#)
[View Journal](#) | [View Issue](#)Cite this: *Dalton Trans.*, 2022, **51**,
7268Received 10th April 2022,
Accepted 20th April 2022

DOI: 10.1039/d2dt01106a

rsc.li/daltonThermal stability and structural studies on the
mixtures of $\text{Mg}(\text{BH}_4)_2$ and glymes†Noemi Leick,^a Ba L. Tran,^{a,c} Mark E. Bowden,^c Thomas Gennett^{a,b} and
Tom Autrey^c

Coordination complexes of $\text{Mg}(\text{BH}_4)_2$ are of interest for energy storage, ranging from hydrogen storage in BH_4 to electrochemical storage in Mg based batteries. Understanding the stability of these complexes is crucial since storage materials are expected to undergo multiple charging and discharging cycles. To do so, we examined the thermal stabilities of the 1 : 1 mixtures of $\text{Mg}(\text{BH}_4)_2$ with different glymes by DSC–TGA, TPD-MS and powder XRD analysis. Despite their structural similarities, these mixtures show diverse phase transitions, speciations and decomposition pathways as a function of linker length.

Introduction

The generation of H_2 from renewable energy provides a pathway toward a decarbonized, sustainable future.¹ Overcoming the intermittency of renewable sources by safe, long-duration storage of H_2 in a compact and efficient form compared to gaseous or cryogenic liquid H_2 remains a major challenge.² A reversible cycle between $\text{Mg}(\text{BH}_4)_2$ and MgB_2 has attracted considerable attention due to a high gravimetric storage density (*ca.* 14.7 wt% H_2) and an ideal thermodynamic range for H_2 release and H_2 uptake at moderate pressure and temperature, ΔG° *ca.* 5 kJ mol^{−1} H_2 .^{3–7} Notwithstanding these attributes, a major drawback is the slow rate of H_2 release of neat, uncomplexed solid $\text{Mg}(\text{BH}_4)_2$ requiring temperatures >250 °C.⁸

Introducing organic additives and transition metals have helped lower the temperature of dehydrogenation.^{9–12} We have shown that adding simple ethereal additives, such as THF and glymes to $\text{Mg}(\text{BH}_4)_2$ can promote dehydrogenation of $\text{Mg}(\text{BH}_4)_2$ at temperatures <200 °C with high selectivity of $\text{B}_{10}\text{H}_{10}^{2-}$ over $\text{B}_{12}\text{H}_{12}^{2-}$ and B_3H_8^- .^{13,14} The product selectivity of $\text{B}_{10}\text{H}_{10}^{2-}$ and $\text{B}_{12}\text{H}_{12}^{2-}$ in the dehydrogenation of $\text{Mg}(\text{BH}_4)_2$ is highly dependent on the glyme-to- $\text{Mg}(\text{BH}_4)_2$ ratio and the identity of the glyme. In addition to H_2 storage, various

$\text{Mg}(\text{BH}_4)_2$ ·glyme mixtures have also garnered interest for Mg batteries because of the stability of BH_4^- anion under reductive conditions, higher natural abundance of Mg and B, increased safety by minimizing dendrite formation and higher energy density of Mg- compared to Li-batteries.^{15–18} Moreover, Mg complexes containing boron clusters¹⁹ or different anions stabilized by glymes^{20–22} have also been examined for battery electrolytes.

A molecular understanding of the interaction between glymes and $\text{Mg}(\text{BH}_4)_2$, and potential degradation pathways of these mixtures are experimentally lacking, yet crucial for materials development.²³ In this report, we investigated the thermal stability and speciation of the mixtures of glymes and $\text{Mg}(\text{BH}_4)_2$ by examining the series of 1 : 1 $\text{Mg}(\text{BH}_4)_2$ ·glyme mixtures by differential scanning calorimetry (DSC), thermogravimetric analysis (TGA) and temperature programmed desorption coupled with quadrupole mass spectrometry (TPD-MS). The combination of these experimental approaches provides insight into both the physical and chemical changes as well as the volatile and non-volatile products formed.

Results and discussion

Phase transitions of the 1 : 1 mixtures of $\text{Mg}(\text{BH}_4)_2$ ·Gn (*n* = 1: monoglyme, 2: diglyme, 3: triglyme and 4: tetraglyme), determined by DSC and TGA, are presented in Fig. 1. The $\text{Mg}(\text{BH}_4)_2$ ·G1 data, collected in a closed system, shows an exotherm at ~60 °C and intense endotherms at ~100 °C and ~110 °C, which most likely results from melting of the mixture. A similar melting process at 100 °C was observed for $\text{Mg}(\text{BH}_4)_2$ ·0.5THF (Fig. S1†). The collection of the DSC data of $\text{Mg}(\text{BH}_4)_2$ ·G1 in an open system shows similar exothermic and endothermic phase transitions that those of the closed system

^aNational Renewable Energy Laboratory, 15013 Denver W Pkwy, Golden, Colorado 80401, USA^bChemistry Department, Colorado School of Mines, 1012 14th Street, Golden, Colorado 80401, USA^cPacific Northwest National Laboratory, Richland, Washington 99354, USA.E-mail: ba.tran@pnnl.gov† Electronic supplementary information (ESI) available: Details of sample preparation, XRD, TGA, and TPD-MS data collection. See DOI: <https://doi.org/10.1039/d2dt01106a>

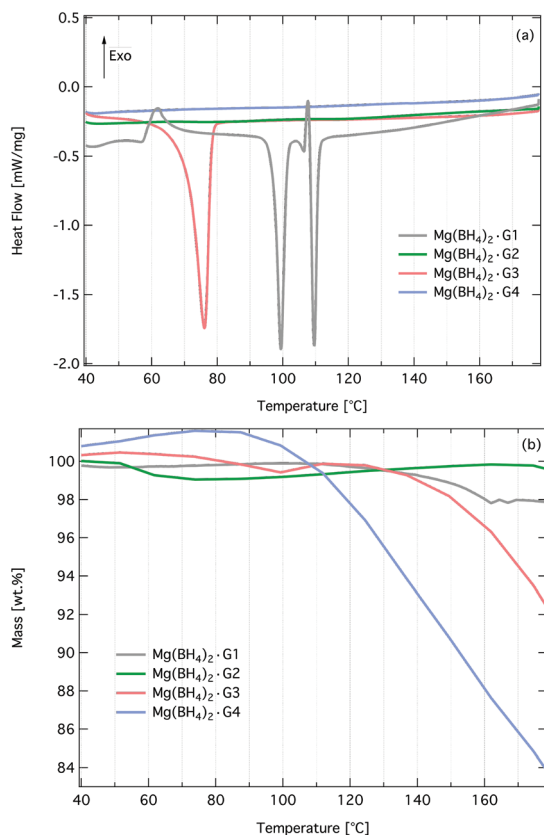


Fig. 1 Mass normalized heat flow as a function of temperature obtained from the closed system of DSC (a) and TGA (b) data for 1 : 1 mixtures of glymes– $\text{Mg}(\text{BH}_4)_2$. G1 = monoglyme, G2 = diglyme, G3 = triglyme, G4 = tetraglyme. Collection parameters: 5°C min^{-1} to 180°C .

(Fig. S2†). We further compared the phase transitions of 1 : 1 mixture of $\text{Mg}(\text{BH}_4)_2$ -G1 to those of pure $\text{Mg}(\text{BH}_4)_2$ ^{12,24} (Fig. S3†) and $\text{Mg}(\text{BH}_4)_2$ -1.5G1,²⁵ which are the major species in the 1 : 1 mixture of $\text{Mg}(\text{BH}_4)_2$ -G1 evidenced by powder XRD analysis (see below). DSC data of $\text{Mg}(\text{BH}_4)_2$ features intense endotherms above 160°C and $\sim 195^\circ\text{C}$ while that of pure $\text{Mg}(\text{BH}_4)_2$ -1.5G1 shows an endotherm at 135°C , which has been attributed to partial loss of G1, and two subsequent exotherms at 250°C and 500°C . From these comparisons, the 1 : 1 $\text{Mg}(\text{BH}_4)_2$ -G1 mixture exhibits drastically different phase transitions at much lower temperatures than that of pure $\text{Mg}(\text{BH}_4)_2$ and $\text{Mg}(\text{BH}_4)_2$ -1.5G1.

In contrast to G1, the DSC data indicates that $\text{Mg}(\text{BH}_4)_2$ -G2 is stable with no phase transitions. The DSC data for $\text{Mg}(\text{BH}_4)_2$ -G3 and $\text{Mg}(\text{BH}_4)_2$ -G4 are also drastically different. A large endotherm ascribed to melting was displayed by $\text{Mg}(\text{BH}_4)_2$ -G3, whereas no phase transitions were observed for $\text{Mg}(\text{BH}_4)_2$ -G4. This was attributed to $\text{Mg}(\text{BH}_4)_2$ -G4 having already become molten before the DSC trace began, and has been confirmed by heating a preparative scale $\text{Mg}(\text{BH}_4)_2$ -G4 to 40°C .

TGA data shows that both $\text{Mg}(\text{BH}_4)_2$ -G3 and $\text{Mg}(\text{BH}_4)_2$ -G4 underwent more mass loss compared to that of $\text{Mg}(\text{BH}_4)_2$ -G1 and $\text{Mg}(\text{BH}_4)_2$ -G2 upon ramping to 180°C . $\text{Mg}(\text{BH}_4)_2$ -G1 and

$\text{Mg}(\text{BH}_4)_2$ -G2 showed negligible mass loss ($<2\%$) compared to that of 9% and 19% for $\text{Mg}(\text{BH}_4)_2$ -G3 and $\text{Mg}(\text{BH}_4)_2$ -G4, respectively. Holding at 180°C for 0.5 h after the ramp gave significant mass losses of 48% was observed for $\text{Mg}(\text{BH}_4)_2$ -G4 and 23% for $\text{Mg}(\text{BH}_4)_2$ -G3 (Fig. S4†). In contrast, $\text{Mg}(\text{BH}_4)_2$ -G1 and $\text{Mg}(\text{BH}_4)_2$ -G2 showed minor mass losses of $<5\%$ upon ramping up to 180°C and holding for 0.5 h (Fig. S4†). The notable mass increase in the TGA data of $\text{Mg}(\text{BH}_4)_2$ -G4 has been reproduced and likely results from the solubility of $\text{Mg}(\text{BH}_4)_2$ in G4 to give a viscous $\text{Mg}(\text{BH}_4)_2$ -G4 that can rapidly interact with ambient species such as O_2 compared to the more crystalline samples of $\text{Mg}(\text{BH}_4)_2$ -G1, $\text{Mg}(\text{BH}_4)_2$ -G2 and $\text{Mg}(\text{BH}_4)_2$ -G3.

We further examined the speciation of 1 : 1 $\text{Mg}(\text{BH}_4)_2$ -G1 by powder XRD and TPD-MS because this mixture selectively produced $\text{B}_{10}\text{H}_{10}^{2-}$ over $\text{B}_{12}\text{H}_{12}^{2-}$.²⁶ Additionally, G1 is commonly employed to ligate Mg^{2+} ions in the development of battery materials.^{15,20,27–29} Powder XRD measurements of 1 : 1 $\text{Mg}(\text{BH}_4)_2$ -G1 were collected at 25°C , 60°C , 70°C (Fig. 2) and 120°C . The preheated mixture of 25°C shows the complex of $[\text{Mg}(\text{G1})_3][\text{Mg}(\text{BH}_4)_4]$ (referred to as $\text{Mg}(\text{BH}_4)_2$ -1.5G1 herein)²⁵ as the major species with minor γ - $\text{Mg}(\text{BH}_4)_2$ starting material. After heating at 60°C for 1 h, the XRD pattern contained $\text{Mg}(\text{BH}_4)_2$ -1.5G1 with significant amounts of unidentified peaks primarily at 8.5° and 6.3° . We have also confirmed that the unidentified peaks are not associated with α - $\text{Mg}(\text{BH}_4)_2$ (Fig. S5†). The formation of crystalline products from $\text{Mg}(\text{BH}_4)_2$ -1.5G1 is consistent with the exotherm at 60°C in the DSC trace. Further heating at 60°C for 6 days transformed the mixture predominantly to $\text{Mg}(\text{BH}_4)_2$ -1.5G1 (Fig. 2A and Fig. S6†) rather than the new unidentified crystalline product

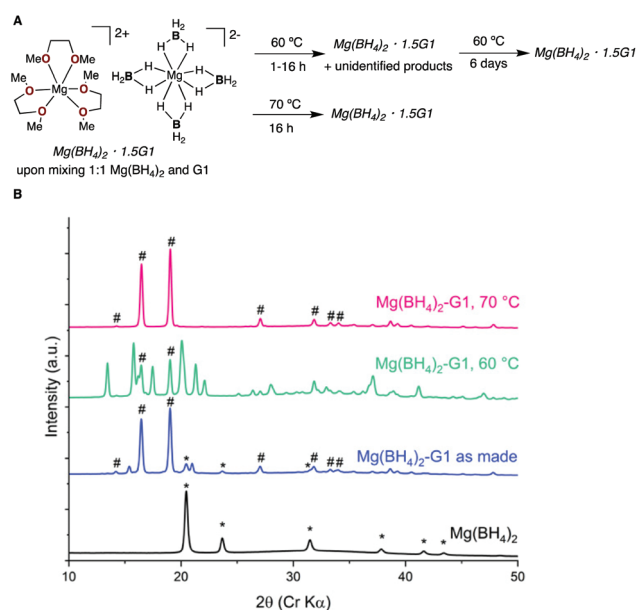


Fig. 2 (A) Summary of powder XRD measurements of the 1 : 1 $\text{Mg}(\text{BH}_4)_2$ -G1 mixture at 25 – 70°C . (B) Powder XRD data of 1 : 1 $\text{Mg}(\text{BH}_4)_2$ -G1 mixture at 25 – 70°C showing the formation of $\text{Mg}(\text{BH}_4)_2$ -1.5G1 (#).



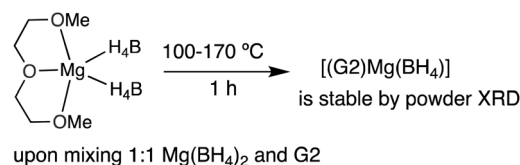
observed at 60 °C at shorter heating time. The reappearance of $\text{Mg}(\text{BH}_4)_2 \cdot 1.5\text{G1}$ at 60 °C (6 days) and 70 °C (16 h) was confirmed by a Rietveld fit of the pattern which showed excellent agreement with that calculated from the structure published by Grochala and co-workers (Fig. S7†).²⁵

To determine whether $\text{Mg}(\text{BH}_4)_2 \cdot 1.5\text{G1}$ exists after the melt, at temperature higher than 100 °C as suggested by DSC data, we heated the 1 : 1 $\text{Mg}(\text{BH}_4)_2 \cdot \text{G1}$ mixture to 120 °C for 1 h leading to melting of the sample to produce a clear glass. Cooling to 25 °C under inert atmosphere gave a transparent product with no evidence of crystalline material. This melting event of 1 : 1 $\text{Mg}(\text{BH}_4)_2 \cdot \text{G1}$ is also corroborated by TPD-MS data (Fig. S8†), in which a major melting linked with the release of more G1 occurs at ~100 °C. Additionally, the $m/z = 2$ signal (H_2) increases but also reveals a noisy signal that usually indicates H_2 transport through a viscous medium, not a solid. Taken together, powder XRD and TPD-MS data support the phase transitions observed in the DSC analysis of 1 : 1 $\text{Mg}(\text{BH}_4)_2 \cdot \text{G1}$.

In a separate study, XRD analysis of single crystals obtained from the reaction of $\text{Mg}(\text{BH}_4)_2$ and 21 equiv. of G1 at 25 °C also showed formation of $\text{Mg}(\text{BH}_4)_2 \cdot 1.5\text{G1}$.²⁵ The formation of $\text{Mg}(\text{BH}_4)_2 \cdot 1.5\text{G1}$, as characterized by solid-state techniques, appears highly favourable for stoichiometric and excess G1 relative to $\text{Mg}(\text{BH}_4)_2$. It is unclear if $\text{Mg}(\text{BH}_4)_2 \cdot 1.5\text{G1}$ is also the predominant species in a solution of $\text{Mg}(\text{BH}_4)_2$ and G1. The isolation and single crystal XRD characterization of $\text{Mg}(\text{BH}_4)_2 \cdot 1.5\text{G1}$ from a solution of $\text{Mg}(\text{BH}_4)_2$ and G1 does not necessarily supplant the proposed solution structure of two neutral $[(\text{G1})\text{Mg}(\text{BH}_4)_2]$ units bridged by G1 in the development of Mg-battery electrolyte.²⁷ These cationic-anionic species should be taken into consideration since similar species to that of $\text{Mg}(\text{BH}_4)_2 \cdot 1.5\text{G1}$ have been structurally characterized from the mixtures of (hexafluoroisopropoxy) borate Ca with G1 and perfluorinated pinacolatoborate Mg with G2 for the development of battery electrolytes.^{20,30} We further showed that a 0.5 M of $\text{Mg}(\text{BH}_4)_2$ in G1 is adequately soluble at ambient temperature as evidenced by observation of strong ^{11}B resonance for BH_4^- against a PhBpin internal standard (Fig. S9†).

Generally, we have observed that additives which induce a melting event, such as THF or G1, are effective for both lowering the temperature and increasing the activity of dehydrogenation. G2 is an anomalously poor additive for the dehydrogenation of $\text{Mg}(\text{BH}_4)_2$ ²⁶ and the lack of a melting event may explains the sluggish dehydrogenation of $\text{Mg}(\text{BH}_4)_2 \cdot \text{G2}$ compared to that of $\text{Mg}(\text{BH}_4)_2 \cdot \text{G1}$ or $\text{Mg}(\text{BH}_4)_2 \cdot 0.5\text{THF}$ by DSC. Therefore, we analysed the preparative-scale thermolysis of 1 : 1 $\text{Mg}(\text{BH}_4)_2 \cdot \text{G2}$ by powder XRD at 100–170 °C (Scheme 1).

The powder XRD data is presented in Fig. S10 of the ESI.† Indeed, heating the 1 : 1 $\text{Mg}(\text{BH}_4)_2 \cdot \text{G2}$ mixture at 100 °C and 170 °C for 1 h did not induce a melt. The crystalline solids of the predominant mononuclear $[(\text{G2})\text{Mg}(\text{BH}_4)_2]$ species, which has been structurally characterized, remained stable at 25 °C, 100 °C and 170 °C.³¹ Moreover, XRD studies clearly show that the complexation of $\text{Mg}(\text{BH}_4)_2$ with G1 or G2 produce funda-



Scheme 1 Powder XRD studies indicate high thermal stability of $[(\text{G2})\text{Mg}(\text{BH}_4)_2]$ to support the lack of phase transitions in the DSC data for 1 : 1 $\text{Mg}(\text{BH}_4)_2 \cdot \text{G2}$.

mentally different species (Fig. 2A and Scheme 1). Additional ^{11}B NMR analysis of the dehydrogenation of 1 : 1 $\text{Mg}(\text{BH}_4)_2 \cdot \text{G2}$ and 1 : 1 $\text{Mg}(\text{BH}_4)_2 \cdot \text{G1}$ at 180–200 °C for 8 h (Fig. S11†) further highlight the effect of G2 and G1 on speciation and thermal stability. The formation of $\text{Mg}(\text{B}_{10}\text{H}_{10})$ (30%) was observed for 1 : 1 $\text{Mg}(\text{BH}_4)_2 \cdot \text{G1}$ at 180 °C for 8 h whereas 1 : 1 $\text{Mg}(\text{BH}_4)_2 \cdot \text{G2}$ requires heating at 200 °C for 8 h to form trace amounts (<5%) of $\text{Mg}(\text{B}_{10}\text{H}_{10})$ (Fig. S11†).

The mass losses from $\text{Mg}(\text{BH}_4)_2 \cdot \text{G3}$ and $\text{Mg}(\text{BH}_4)_2 \cdot \text{G4}$ are not simply volatile G3 (MP = 216 °C) and G4 (MP = 275 °C) as evidenced by their different mass spectrometry (MS) fragmentation patterns compared to free G4 or G3 (Fig. 3 and

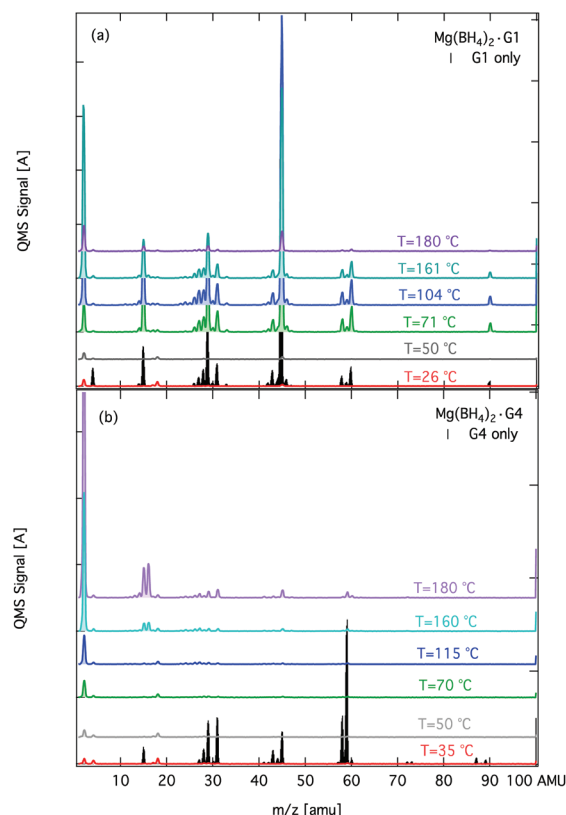


Fig. 3 Signal from the QMS in the m/z range of 1–100 amu recorded during heating of (a) $\text{Mg}(\text{BH}_4)_2 \cdot \text{G1}$ and (b) $\text{Mg}(\text{BH}_4)_2 \cdot \text{G4}$. For comparison, the fragmentation pattern of G1 and G4 were recorded and are shown at 26 °C and 47 °C, respectively. The samples were heated at 5 °C min^{-1} to 180 °C.



Fig. S12†). This observation suggests that the complexation to the Mg^{2+} ion plausibly mediates the decomposition of G3 and G4. Therefore, to understand potential decomposition pathways of these mixtures, we analysed the volatiles at different temperatures by MS. A summary of the MS data of $\text{Mg}(\text{BH}_4)_2\cdot\text{G1}$ and $\text{Mg}(\text{BH}_4)_2\cdot\text{G4}$ is shown in Fig. 3 and those of $\text{Mg}(\text{BH}_4)_2\cdot\text{G2}$ and $\text{Mg}(\text{BH}_4)_2\cdot\text{G3}$ are in Fig. S12.† It appears that the volatile products may depend on the linker in the glyme.

Specifically, the fragmentation pattern of the volatiles from the thermolysis of $\text{Mg}(\text{BH}_4)_2\cdot\text{G1}$ resembles that of free G1 at 26 °C. In stark contrast, the fragmentation of volatiles of $\text{Mg}(\text{BH}_4)_2\cdot\text{G4}$ is different from that of free G4 at 35 °C. For example, the fragmentation pattern of $\text{Mg}(\text{BH}_4)_2\cdot\text{G4}$ at 50 °C is distinct from that of free G4 (Fig. 3). We observe the appearance of $m/z = 15, 16$ above 160 °C, which potentially corresponds to methane release from the demethylation of G4 in the $\text{Mg}(\text{BH}_4)_2\cdot\text{G4}$ complex. The fragmentation pattern of $\text{Mg}(\text{BH}_4)_2\cdot\text{G3}$ is a mix between that of $\text{Mg}(\text{BH}_4)_2\cdot\text{G1}$ and $\text{Mg}(\text{BH}_4)_2\cdot\text{G4}$ in that the volatiles consist of glyme units and methane at 183 °C (Fig. S12†). The results of MS analysis suggest that longer glymes, like G3 and G4, can undergo irreversible demethylation.

^{11}B NMR analysis after the thermolysis of 1 : 1 $\text{Mg}(\text{BH}_4)_2\cdot\text{G4}$ at 180 °C for 8 h produced $\text{Mg}(\text{B}_{10}\text{H}_{10})$, $\text{Mg}(\text{B}_{12}\text{H}_{12})$ and unreacted $\text{Mg}(\text{BH}_4)_2$ without evidence of B–O products (Fig. S13†). The lack of a B–O product from $\text{Mg}(\text{BH}_4)_2$ and a linear ether (*i.e.* G4) compared to that of B–O product formation in a cyclic ether (*i.e.* THF) by a plausible ring opening further highlights the different chemical reactivity of the different ethereal additives. This also suggests that Mg-alkoxide species may form instead of B–O products.³² Unfortunately, subsequent powder XRD analysis of the post-reaction mixture was uninformative because the mixture was amorphous (Fig. S14†). It is plausible that the dynamic flexibility of the longer glymes compared to that of shorter glymes can lead to different conformations, thus contributing to different degradation pathways such as demethylation. The demethylation of $\text{Mg}(\text{BH}_4)_2\cdot\text{G3}$ and $\text{Mg}(\text{BH}_4)_2\cdot\text{G4}$ at elevated temperatures may pose limitations on the use of these mixtures for multiple cycling processes required for an energy storage material.

Summary

By combining a suite of analytical techniques, we have shown that the 1 : 1 mixtures of $\text{Mg}(\text{BH}_4)_2\cdot\text{Gn}$ ($n = 1\text{--}4$) display notably different phase transitions and speciations, ranging from melts at low temperatures to compounds, such as $\text{Mg}(\text{BH}_4)_2\cdot\text{G2}$, which are highly stable up to 180 °C. TPD-MS analysis provided evidence of H_2 release, different fragmentation, and volatiles as a function of the glyme chain length. Observation of irreversible methane release from mixtures of $\text{Mg}(\text{BH}_4)_2\cdot\text{G4}$ and $\text{Mg}(\text{BH}_4)_2\cdot\text{G3}$ at operating conditions for $\text{Mg}(\text{BH}_4)_2$ dehydrogenation, which are absent for $\text{Mg}(\text{BH}_4)_2\cdot\text{G1}$ and $\text{Mg}(\text{BH}_4)_2\cdot\text{G2}$, offers insight into the chemical stabilities of

employing $\text{Mg}(\text{BH}_4)_2$ -glymes mixtures for the development of additives for energy storage materials.

Experimental section

General considerations

All materials were purchased, stored in a N_2 glovebox and used as is unless otherwise noted. $\text{Mg}(\text{BH}_4)_2$ (1.0 g, 95%) was sourced from Sigma Aldrich. All glymes (G1, G2, G3, G4) were dried over CaH_2 with vigorous stirring over 48 h, purified by distillation and stored over activated 4 Å molecular sieves in a nitrogen glove box. The heat flow measurements of the glymes only and the $\text{Mg}(\text{BH}_4)_2$ -glyme mixtures were performed using differential scanning calorimetry (DSC) on a Q20 TA Instrument DSC. The samples were heated from 25 to 180 °C at a rate of 5 °C min^{-1} in a N_2 atmosphere. The samples were enclosed in hermetically sealed Tzero aluminium pans prepared in a He glovebox, which necessitated the use of a reference pan prepared in a He atmosphere as well. For the collection of the open-system DSC-TGA data, the samples were prepared in an uncapped crucible inside an N_2 glovebox, loaded in the instrument and flushed with N_2 . The data were obtained by heating the samples under N_2 gas from 25 to 180 °C at a rate of 5 °C min^{-1} . The samples studied for this work were analyzed on a calibrated, custom-built thermal programmed desorption (TPD) system equipped with a Stanford Research Systems RGA 100, with $m/z = 1\text{--}100$ amu, sampling rate of 4 seconds and 70 eV ionization energy. The samples were heated at a rate of 5 °C min^{-1} from 26 to 180 °C utilizing a Digi-Sense temperature controller. The quantity of material was adjusted to stay within the calibrated mass spectrometer's linear response region. In a typical analysis, 2–10 mg of sample was placed inside a quartz tube mounted to the TPD system. All experimental parameters were controlled *via* a LabView™ interface with the RGA, heating system, and pressure gauges. Typical initial pressures before heating the sample are at 10^{-8} Torr, with a flat baseline, *i.e.* no water, hydrogen or air signals above background. Further information on the system was previously published.³³

For powder XRD characterization, the solids were transferred to a glass capillary (500 µm diameter, 10 µm wall thickness, Charles Supper Co., MA) and sealed using wax and a wax pen inside an N_2 glovebox. A Rigaku D/Max Rapid II micro diffraction system with a rotating Cr target ($\lambda = 2.2910$ Å) operated at 35 kV and 25 mA was used to collect the diffraction patterns. A parallel X-ray beam collimated to 300 µm diameter was directed onto the specimen and the diffracted intensities were recorded on a large 2D image plate over a 10 minute exposure. The 2D images were integrated between 10 and 150° 2θ to give standard powder traces. ^{11}B NMR characterization of the boron products in the dehydrogenation reactions were recorded in 2 : 1 $\text{D}_2\text{O} : \text{THF}$. All additional ^{11}B NMR, DSC, TGA, TPD, MS and GC-MS data are provided in the ESI.†



General procedure for the preparation and thermolysis of 1 : 1 Mg(BH₄)₂ : glymes mixtures

Inside a nitrogen-filled glovebox, to a 3 mL oven-dried scintillation vial was added solid Mg(BH₄)₂ (20.0 mg, 0.370 mmol) and glyme (0.370 mmol) by microsyringe. The resulting solid mixture was thoroughly mixed and repeatedly smeared against the wall using a spatula. The resulting mixture was transferred to a 25 mL Schlenk tube. The closed Schlenk tube was placed in a preheated aluminum block at the different temperatures and reaction time for the different experiments. The resulting mixture was returned to the glovebox and all manipulation and preparation of the sample for subsequent characterization were performed under inert atmosphere inside the glovebox.

Conflicts of interest

The authors declare no conflict of interest.

Acknowledgements

We acknowledge the Hydrogen Materials-Advanced Research Consortium (HyMARC), established as part of the Energy Materials Network under the U.S. Department of Energy, Office of Energy Efficiency and Renewable Energy, Hydrogen and Fuel Cell Technologies Office (Contract No. DE-AC36-08GO28308), Environmental Molecular Sciences Laboratory (award 10.46936/cpcy.proj.2020.51656/60000242), a DOE Office of Science User Facility sponsored by the Biological and Environmental Research under Contract No. DE-AC05-76RL01830 for research support. The authors thank C. M. Jensen for insightful discussions. Pacific Northwest National Laboratory is operated by Battelle for the U.S. Department of Energy.

Notes and references

- N. S. Lewis and D. G. Nocera, *Proc. Natl. Acad. Sci. U. S. A.*, 2006, **103**, 15729–15735.
- B. Sakintuna, F. Lamaridarkrim and M. Hirscher, *Int. J. Hydrogen Energy*, 2007, **32**, 1121–1140.
- Y. Filinchuk, B. Richter, T. R. Jensen, V. Dmitriev, D. Chernyshov and H. Hagemann, *Angew. Chem., Int. Ed.*, 2011, **50**, 11162–11166.
- O. Zavorotynska, A. El-Kharbach, S. Deledda and B. C. Hauback, *Int. J. Hydrogen Energy*, 2016, **41**, 14387–14403.
- G. Soloveichik, Y. Gao, J. Rijssenbeek, M. Andrus, S. Kniajanski, R. Bowmanjr, S. Hwang and J. Zhao, *Int. J. Hydrogen Energy*, 2009, **34**, 916–928.
- Y. Zhang, E. Majzoub, V. Ozoliņš and C. Wolverton, *J. Phys. Chem. C*, 2012, **116**, 10522–10528.
- I. H. Nayyar, B. Ginovska, M. Bowden, G. Edverson, B. Tran and T. Autrey, *J. Phys. Chem. A*, 2022, **126**, 444–452.
- N. P. Stadie, E. Callini, B. Richter, T. R. Jensen, A. Borgschulte and A. Züttel, *J. Am. Chem. Soc.*, 2014, **136**, 8181–8184.
- J. Chen, Y. S. Chua, H. Wu, Z. Xiong, T. He, W. Zhou, X. Ju, M. Yang, G. Wu and P. Chen, *Int. J. Hydrogen Energy*, 2015, **40**, 412–419.
- S. Zhao, B. Xu, N. Sun, Z. Sun, Y. Zeng and L. Meng, *Int. J. Hydrogen Energy*, 2015, **40**, 8721–9731.
- E. G. Bardají, N. Hanada, O. Zabara and M. Frichtner, *Int. J. Hydrogen Energy*, 2011, **36**, 12313–12318.
- N. Leick, N. A. Strange, A. Schneemann, V. Stavila, K. Gross, N. Washton, A. Settle, M. B. Martinez, T. Gennett and S. T. Christensen, *ACS Appl. Energy Mater.*, 2021, **4**, 1150–1162.
- M. Chong, T. Autrey and C. Jensen, *Inorganics*, 2017, **5**, 89.
- M. Chong, A. Karkamkar, T. Autrey, S. Orimo, S. Jalisatgi and C. M. Jensen, *Chem. Commun.*, 2011, **47**, 1330–1332.
- Y. Shao, N. N. Rajput, J. Hu, M. Hu, T. Liu, Z. Wei, M. Gu, X. Deng, S. Xu, K. S. Han, J. Wang, Z. Nie, G. Li, K. R. Zavadil, J. Xiao, C. Wang, W. A. Henderson, J.-G. Zhang, Y. Wang, K. T. Mueller, K. Persson and J. Liu, *Nano Energy*, 2015, **12**, 750–759.
- T. Burankova, E. Roedern, A. E. Maniadaki, H. Hagemann, D. Rentsch, Z. Lodziana, C. Battaglia, A. Remhof and J. P. Embs, *J. Phys. Chem. Lett.*, 2018, **9**, 6450–6455.
- D. Samuel, C. Steinhäuser, J. G. Smith, A. Kaufman, M. D. Radin, J. Naruse, H. Hiramatsu and D. J. Siegel, *ACS Appl. Mater. Interfaces*, 2017, **9**, 43755–43766.
- R. Mohtadi, M. Matsui, T. S. Arthur and S.-J. Hwang, *Angew. Chem., Int. Ed.*, 2012, **51**, 9780–9783.
- R. Mohtadi, *Molecules*, 2020, **25**, 1791–1816.
- J. Luo, Y. Bi, L. Zhang, X. Zhang and T. L. Liu, *Angew. Chem., Int. Ed.*, 2019, **58**, 6967–6971.
- S. Hebié, H. P. K. Ngo, J.-C. Leprêtre, C. Iojoiu, L. Cointeaux, R. Berthelot and F. Alloin, *ACS Appl. Mater. Interfaces*, 2017, **9**, 28377–28385.
- N. Sa, N. N. Rajput, H. Wang, B. Key, M. Ferrandon, V. Srinivasan, K. A. Persson, A. K. Burrell and J. T. Vaughney, *RSC Adv.*, 2016, **6**, 113663–113670.
- N. N. Rajput, X. Qu, N. Sa, A. K. Burrell and K. A. Persson, *J. Am. Chem. Soc.*, 2015, **137**, 3411–3420.
- I. Saldan, *Int. J. Hydrogen Energy*, 2016, **41**, 11201–11224.
- W. Wegner, T. Jaron, M. A. Dobrowolski, L. Dobrzycki, M. K. Cyranski and W. Grochala, *Dalton Trans.*, 2016, **45**, 14370–14377.
- B. L. Tran, T. N. Allen, M. E. Bowden, T. S. Autrey and C. M. Jensen, *Inorganics*, 2021, **9**, 41.
- Y. Shao, T. Liu, G. Li, M. Gu, Z. Nie, M. Engelhard, J. Xiao, D. Lv, C. Wang, J. G. Zhang and J. Liu, *Sci. Rep.*, 2013, **3**, 3130.
- S. Hou, X. Ji, K. Gaskell, P.-f. Wang, L. Wang, J. Xu, R. Sun, O. Borodin and C. Wang, *Science*, 2021, **374**, 172–178.
- Y. Bi, S. He, C. Fan, J. Luo, B. Yuan and T. L. Liu, *J. Mater. Chem. A*, 2020, **8**, 12301–12305.
- K. V. Nielson and T. L. Liu, *Angew. Chem., Int. Ed.*, 2020, **59**, 3368–3370.
- M. V. Solovev, O. V. Chashchikhin, P. V. Dorovatovskii, V. N. Khrustalev, A. S. Zyubin, T. S. Zyubina,



- O. V. Kravchenko, A. A. Zaytsev and Y. A. Dobrovolsky, *J. Power Sources*, 2018, **377**, 93–102.
- 32 See the ESI.† Acidification and GC-MS characterization of the post-thermolysis reaction of 1 : 1 $\text{Mg}(\text{BH}_4)_2$ -G4 showed G4 and three new species (Table S1, pp. S12–S14†) containing similar fragmentation patterns.
- 33 K. E. Hurst, M. J. Heben, J. L. Blackburn, T. Genett, A. C. Dillon and P. A. Parilla, *Rev. Sci. Instrum.*, 2013, **84**, 025103.

